https://doi.org/10.5194/egusphere-2026-2679
Preprint. Discussion started: 21 May 2026

Calcium carbonate dissolution rate changes under future climate scenarios

David Samuel Trossman[1]
[1]National Oceanography Centre, 6 Brownlow Street, Liverpool L3 5DA, UK

Correspondence: David Samuel Trossman (david.trossman@noc.ac.uk)

Abstract. Calcium carbonate is known to be dissolving throughout various portions of the water column, but little is known about how this will change in the future. Model output of a large range of climate scenarios and an established diagnostic approach are used to understand the future of calcium carbonate dissolution rates. Changes in ocean salinity and mean age are of leading order importance to future calcium carbonate dissolution rates. The calcium carbonate dissolution rates can range by an order of magnitude across climate scenarios in regions such as the subtropical Atlantic Ocean basins. Some geoengineering methods are more effective than others at decreasing calcium carbonate dissolution rates in particular regions of the ocean; however, no single technique is effective everywhere. Altered calcium carbonate dissolution rates have implications for the physical ocean state projections, such as those for sea level, which are discussed in terms of direct and indirect impacts. Direct impacts due to the presence of suspended sediments comprised of calcium carbonate can be significant in some river deltas and nearby coasts.

1 Introduction

Calcium carbonate dissolution regulates atmospheric carbon dioxide levels by playing an important role in the ocean's carbon and alkalinity cycles. The ultimate fate of anthropogenically generated carbon that reaches the seafloor on multi-millennial time scales is calcium carbonate dissolution (Archer et al. , 2009). The excess alkalinity in the ocean interior relative to the sea surface along an isopyncal is due to the dissolution of calcium carbonate (Feely et al. , 2004). Seawater saturation is the main control on calcium carbonate dissolution (Wu et al. , 2025), with significant calcium carbonate dissolution in supersaturated waters (Sulpis et al. , 2021), but in the upper-ocean, calcium carbonate dissolution is sensitive to ocean export production, which helps the ocean retain more carbon dioxide (Kwon et al. , 2024). Since pre-industrial times, seafloor calcium carbonate dissolution rates have likely increased (Sulpis et al. , 2018). However, little is known about how calcium dissolution rates will change (throughout the water column) in the future.

Future changes in calcium carbonate dissolution rates could have important implications for climate over the next several decades. The dissolution of calcium carbonate in the ocean does not only concern about 40% of sediments (e.g., Nworie et al. (2026)); it also includes the shells of marine species as well as other marine biota and material (e.g., Goossens et al. (2026)). Calcium carbonate dissolution in shallow environments, including the shelves, is a significant fraction (nearly 10%) of the global carbonate dissolution (Goossens et al. , 2026). On the shelves, the dissolution of calcium carbonate-based sediments

https://doi.org/10.5194/egusphere-2026-2679
Preprint. Discussion started: 21 May 2026

could constitute part of a climate feedback acting on annual-to-decadal time scales that accounts for about 10% of the missing carbon in carbon budgets of ocean models (van deVelde et al. , 2026). It is difficult to predict how much of this carbon will remain in the ocean due to a complex interplay of physical and biogeochemical processes (Gillett , 2023). Therefore, accounting for changes in calcium carbonate dissolution rates over the next several decades will likely be necessary to accurately simulate oceanic sources and sinks of carbon dioxide, particularly in application to marine carbon dioxide removal attempts.

In the present study, we evaluate the sensitivity of calcium carbonate dissolution to various factors using climate model output under multiple future scenarios, including ones that have large-scale implementation of geoengineering technologies. There are multiple methods to estimate calcium carbonate dissolution rates, including the diagnostic approach based on a suite of ocean tracers with observationally derived data products (e.g., Sulpis et al. (2021)) and an inverse modeling approach to account for cross-isopycnal transports and mixing (e.g., Wu et al. (2025)). Because of the prohibitive computational resources needed to construct climate states (over ~ 30 years) using an inverse model approach and difficulty with quantifying the resulting propagated uncertainties under multiple future scenarios, we use the diagnostic approach of Sulpis et al. (2021) to get a first-order understanding of how calcium carbonate dissolution rates will change in the future. Climate model output is used as a perturbation to the observationally derived data products used in Sulpis et al. (2021). We will discuss the potential implications of these findings with respect to the future physical ocean state, including sea level.

2 Methods

In this study, we calculate the calcium carbonate dissolution rate changes using the same potential alkalinity-based method that Sulpis et al. (2021) employed, but instead of performing the calculations over pre-industrial times we apply perturbations to several variables that could influence calcium carbonate dissolution under future climate scenarios. The slope of the Alk*-age linear relationship divided by 2 gives the calcium carbonate dissolution rate, where Alk* is the potential alkalinity defined by Carter et al. (2014) as:

$$Alk* = TA + 1.26[NO_3^-] - 66.4S, \tag{1}$$

where TA is the titration alkalinity (calculated with CO2SYS (van Heuven et al. , 2011)), $[NO_3^-]$ is the nitrate concentration, and S is the salinity. The age used in the calculations uses a combination of transit time distribution-based mean ages (Jeansson et al. , 2021) up to 200 years and Carbon-14-based mean ages (Gebbie and Huybers , 2012) above 300 years, with a linear transition between 200-300 years. For each region we consider (Fay and McKinley , 2014), Alk* and age data were sorted according to increasing potential density and then placed into density bins. For each density bin, we fit Alk* versus age via linear regression and extracted the slope. Uncertainties were propagated using a Monte Carlo approach, where the density increment randomly varied between 0.002 and 0.05, the age uncertainty was set at 20%, and the Alk* uncertainty was 6 μmol kg^{-1}. A cubic smoothing spline was used for vertical interpolation. Our results in the open ocean should be approximately within model projection accuracy because calcium carbonate dissolution in the deeper ocean is mostly determined by the thermodynamics of calcium carbonate saturation (Kwon et al. , 2024).

https://doi.org/10.5194/egusphere-2026-2679
Preprint. Discussion started: 21 May 2026

We first focus on temperature, salinity, mean age, and dissolved oxygen concentrations in the final 30 years of the 21st century relative to those in the first 30 years of the same century based on CMIP6 model output under the SSP5-8.5 scenario, documented in Guo et al. (2026). We do not perform an assessment of the CMIP6 output with the GLODAPv2 data that Sulpis et al. (2021) used because the CMIP6 control simulations are for pre-industrial times and the GLODAPv2-derived product is a particularly sampling and interpolation of conditions over the past few decades. Additionally, the mean ages from model output are from ideal age tracers, which are similar but not the same as the transit-time distribution-based ages (Guo et al. , 2025). Mean ages reflect changes in ocean ventilation (e.g., Gnanadesikan et al (2007); Khatiwala et al. (2012)). These CMIP6-based estimates are considered upper-bounds for future projections. To find the lower-bounds for future projections, we use output from GeoMIP scenarios that include the same four variables. These simulations additionally include nitrate, phosphate, alkalinity, and total carbon (whose perturbations are assumed to be entirely comprised of DIC because that is the only contribution available in the output) so we can assess the sensitivities of calcium carbonate dissolution rates to these variables as well. The CMIP6-based estimates can likely neglect the perturbations to the four biogeochemical variables that are included in the GeoMIP output because, as it will be shown later, the sensitivities of the calcium carbonate dissolution rates to these four biogeochemical variables are relatively small. The GeoMIP scenarios were documented by Oschlies et al. (2025) and include interventions such as artificial upwelling, macroalgae farming with biomass harvesting and storage outside the ocean, macroalgae farming and sinking with only the Redfield portion of sunk biomass remineralized and the excess organic carbon left non-remineralized, macroalgae farming and sinking with complete remineralization after 90 years of continuous deployment from year 2020–2110, ocean alkalinity enhancement, and ocean iron fertilization south of $30^o S$ (in the Southern Ocean). Only two GeoMIP scenarios include Carbon-14 output for us to be able to infer an age perturbation (albeit only above 300 years): artificial upwelling and ocean iron fertilization in the Southern Ocean. We show results from the artificial upwelling scenario as examples throughout most of our GeoMIP-based analysis because the Carbon-14 values in the iron fertilization in the Southern Ocean scenario are generally outside of the range to compute mean ages from the empirical relationship (Gebbie and Huybers , 2012):

$$\tau = -8267(ln(\Delta C_{14,ctrl}/\Delta C_{14,future}) - ln(1)), \quad (2)$$

where τ is the mean age, $\Delta C_{14,ctrl}$ is the Carbon-14 from the control simulation, and $\Delta C_{14,future}$ is the Carbon-14 from the carbon dioxide perturbation with geoengineering simulation. This empirical relationship has a limited range of applicability, but will be used here to demonstrate how sensitive our estimates of calcium carbonate dissolution rates are to mean ages in the GeoMIP scenarios.

3 Results

3.1 CMIP6

We first inspect the four state variables available from 11 of the CMIP6 simulations under the SSP5-8.5 scenario (Figure 1-top) and their perturbations (2070-2099 average minus 2000-2029 average) (Figure 1-bottom). Mean age, salinity, oxygen,

https://doi.org/10.5194/egusphere-2026-2679
Preprint. Discussion started: 21 May 2026

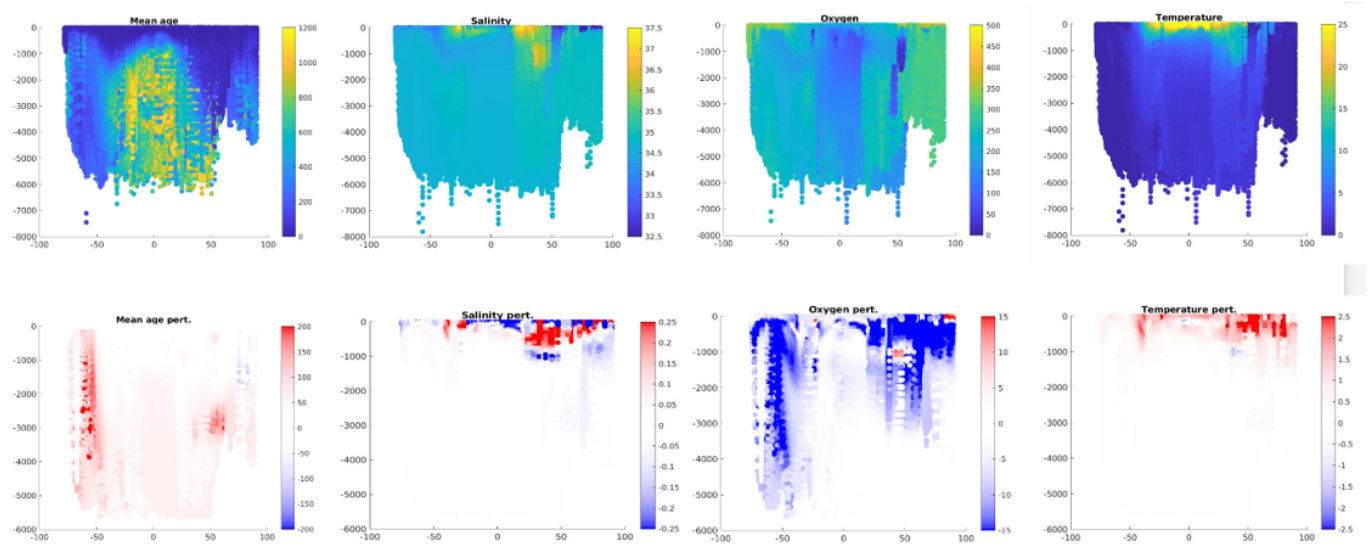

Figure 1. State variables from the control (historical) simulation averaged over 11 different models in the CMIP6 archive and their perturbations at locations and depths where samples are available to compare with GLODAPv2-based estimates of calcium carbonate dissolution rates from Sulpis et al. (2021).

and temperature are sampled like GLODAPv2 data were sampled in Sulpis et al. (2021), which explains much of the spatial patterns in Figure 1. For example, the lower oxygen concentrations near the equator are due to sampling the Pacific and Indian Oceans more than the Atlantic Ocean at those latitudes and the lower mean ages in the northern subpolar regions are due to sampling the Atlantic Ocean more than the other ocean basins at those latitudes. Mean age increases in the Atlantic sector of the Southern Ocean, salinity generally decreases at high-latitudes and increases in more tropical regions (aside from the east coast of Greenland), dissolved oxygen concentrations generally decrease except in a couple of high-latitude regions (e.g., the Pacific sector of the Southern Ocean) and the tropical Indian Ocean, and temperature increases in many regions (particularly at the high northern latitudes) from the beginning of the century to the end (Figure 1-bottom). The temperature and salinity changes are primarily externally forced but underestimated in the North Atlantic Ocean (Molodtsov et al. , 2025), suggesting that our CMIP6-derived calcium carbonate dissolution rates will be underestimated as well. The subtropical Atlantic gyres are expected to get drier and therefore more salty, whereas the subpolar North Atlantic is expected to get fresher, which isn't fully represented because ice sheets are not dynamically coupled with the rest of the components of climate models and this likely inadequately simulates the freshening of the oceans as well as many teleconnections (e.g., Testorf et al. (2026)). These results will be contrasted with GeoMIP output in the following section.

We next examine how the calcium carbonate dissolution rates change when adjusting all four of these factors versus one at a time. When all four of the above-listed factors are perturbed simultaneously (Figure 2), the sediment dissolution rates are predicted to most dramatically increase in the subtropical North Atlantic Ocean, with more pronounced changes near the surface. In these regions, each of the three saturation depths (for Mg calcite, aragonite, and calcite) become shallower in

https://doi.org/10.5194/egusphere-2026-2679
Preprint. Discussion started: 21 May 2026

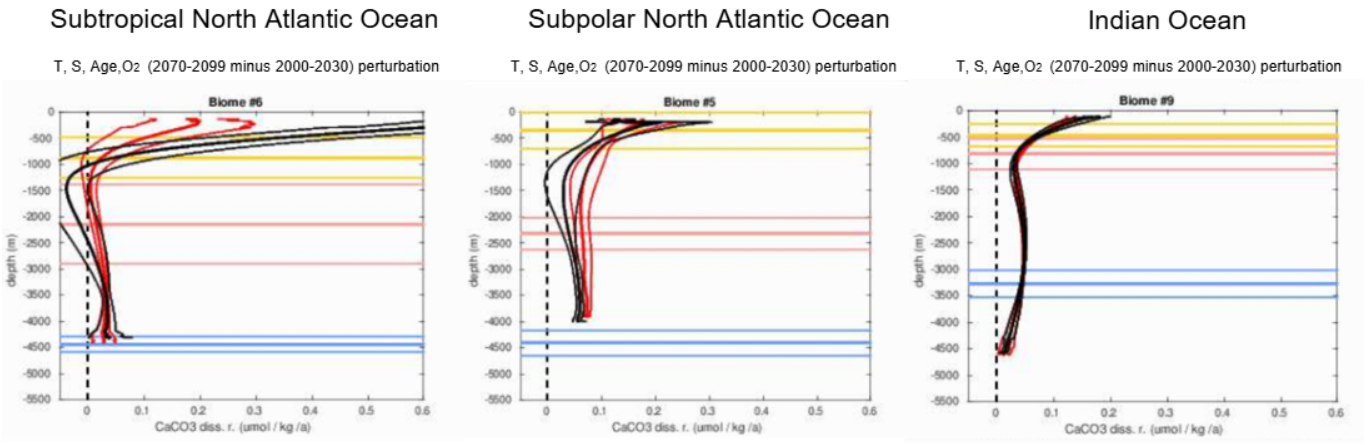

Figure 2. Calcium carbonate dissolution rates for different biomes (Fay and McKinley , 2014) or geographic regions (#9 is the Indian Ocean, #6 is the subtropical North Atlantic, and #5 is the subpolar North Atlantic) with perturbations in temperature (T), salinity (S), age (Age), and dissolved oxygen concentrations (O2) by adding the difference in those variables over the average of the final 30 years of 11 different CMIP6 models minus the first 30 years of the same models to the GLODAPv2-equivalent variables at the locations where they have been sampled. Shown in black are the perturbed estimates with one standard deviation and shown in red are the initial GLODAPv2-derived estimates from Sulpis et al. (2021). The horizontal yellow line is the saturation depth of Mg calcites, the horizontal red line is the saturation depth of aragonite, and the horizontal blue line is the saturation depth of calcite in the perturbed (CMIP6-based) estimate corresponding to the black curves. Monte Carlo-derived standard deviations are also included on these saturation depths.

the future. Recall from Sulpis et al. (2021) that shallow-water dissolution is controlled by metabolic processes (i.e., carbon dioxide produced during animal and/or microbial respiration) and the presence of Mg calcites, whereas deep-water dissolution is determined by the higher solubility of calcium carbonate in bulk solution. The transition depth between these two regimes can be determined by the shallowest depth at which the vertical derivative of the dissolution rate profile vanishes. The sediment dissolution rates (and sinking fluxes-not shown) remain approximately the same in most regions, the exception being the Indian Ocean where they decrease by less than 10%. Salinity has an increasing effect on the dissolution rates in the near-surface and/or mid-depth extra-tropical oceans and a more variable effect in tropical oceans (Figure 3). The impact of salinity on Alk* is apparent through Eq (1); the changes in TA and $[NO_3^-]$ are relatively small compared to salinity, and this gets magnified after scaling those factors by their coefficients in Eq (1) (1, 1.26, and 66.4 to TA, $[NO_3^-]$ and S respectively). The impact of mean age is also straightforward because the dissolution rates are determined by the slope of the Alk*-age relationship. Mean age has a significant decreasing effect on the dissolution rates in the near-surface Southern Ocean and mid-depth subpolar North Atlantic Ocean, with a more variable effect elsewhere (Figure 4). Less obvious is how temperature and oxygen alter the calcium carbonate dissolution rates, but they each have a very small impact (not shown). In summary, salinity and mean age changes dominate the changes in dissolution rates, but other factors can impact Alk* (via $[NO_3^-]$ or the CO2SYS calculation of TA), which can propagate into dissolution rate perturbations.

https://doi.org/10.5194/egusphere-2026-2679
Preprint. Discussion started: 21 May 2026

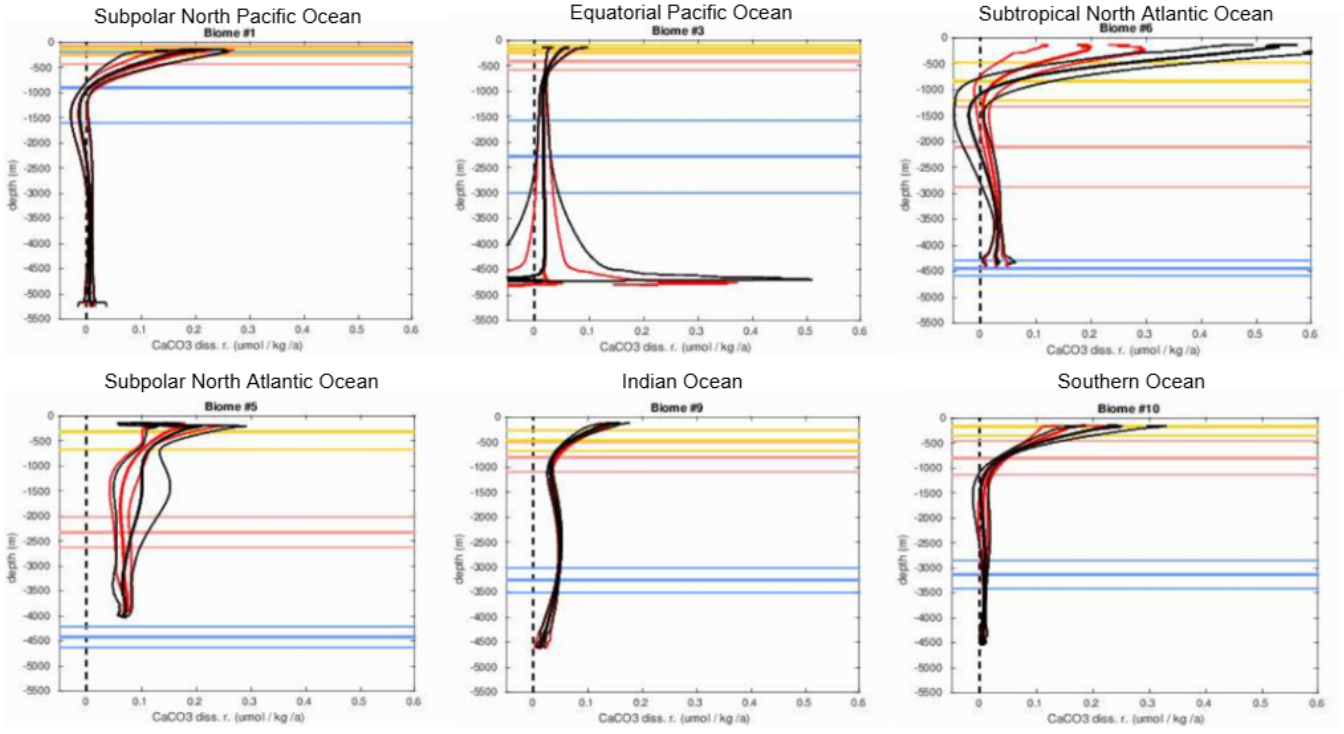

Figure 3. Influence of a perturbation to salinity alone on calcium carbonate dissolution rates in several regions (#10 is the Southern Ocean, #9 is the Indian Ocean, #6 is the subtropical North Atlantic, #5 is the subpolar North Atlantic, #3 is the equatorial Pacific, and #1 is the subpolar North Pacific Oceans). The colors are consistent with Figure 2.

3.2 GeoMIP

The four overlapping variables available from the control simulations associated with any of the GeoMIP scenarios (Figure 5-top) are visually identical to the control simulations of the CMIP6 scenario (Figure 1-top). The remaining four variables from the control simulations associated with one of the GeoMIP scenarios (artificial upwelling) are also shown (Figure 5-bottom); nitrate, phosphate, and total carbon are spatially similar while alkalinity is more uniform in its spatial structure, aside from low values found on the Siberian shelf where we do not attempt to estimate calcium carbonate dissolution rates and at deeper depths outside of the polar regions. Each of the eight variables considered here appear identical in each of the control simulations from the GeoMIP scenarios (not shown).

We focus on the perturbations to the above-mentioned eight variables from the artificial upwelling scenario as an example (Figure 6). The mean age changes are more dramatic in the Southern Ocean iron fertilization scenario due to a general decrease in total carbon (not shown); nitrate and phosphate generally increase, and oxygen concentrations generally decrease in the Southern Ocean under this scenario. The mean ages generally increase under the artificial upwelling scenario, particularly in areas with deep convection and regions that upwell due to the winds already, but primarily in the upper ocean due to mixing

https://doi.org/10.5194/egusphere-2026-2679
Preprint. Discussion started: 21 May 2026

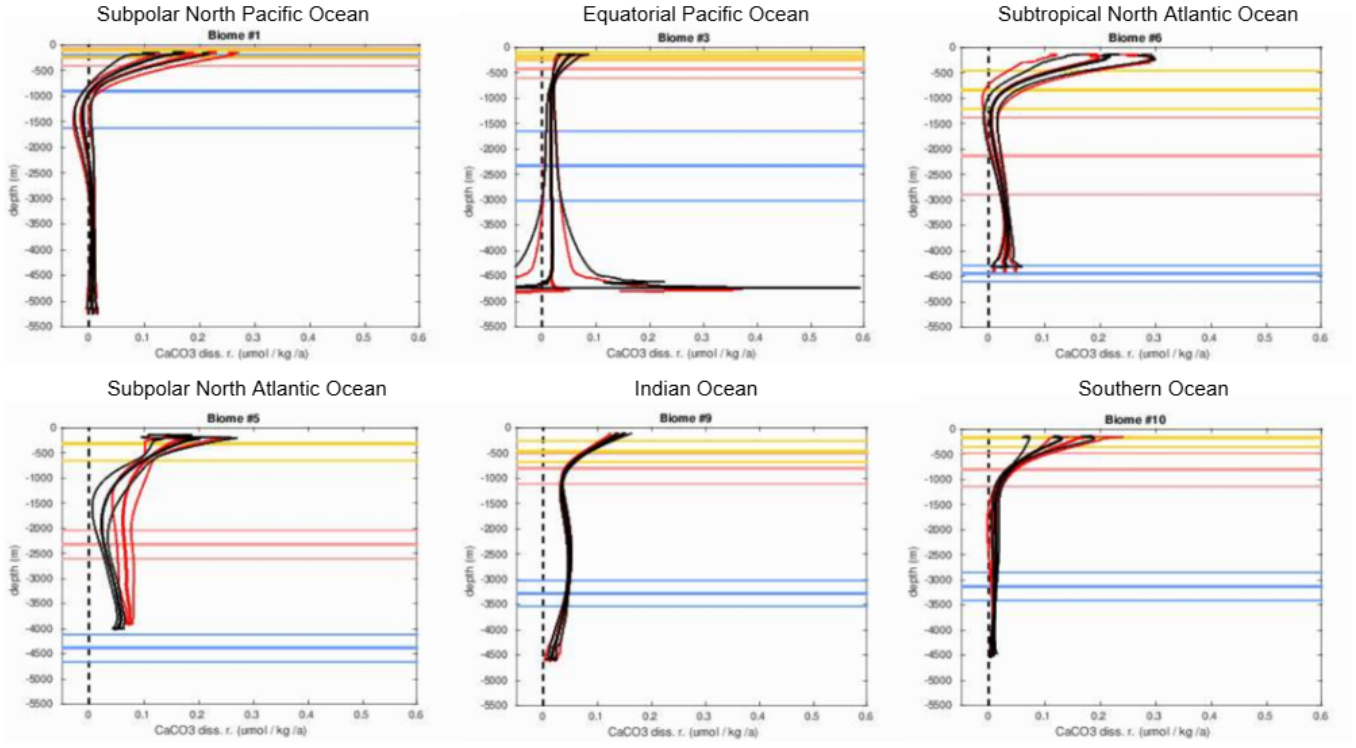

Figure 4. Influence of a perturbation to mean age alone on calcium carbonate dissolution rates in several regions (#10 is the Southern Ocean, #9 is the Indian Ocean, #6 is the subtropical North Atlantic, #5 is the subpolar North Atlantic, #3 is the equatorial Pacific, and #1 is the subpolar North Pacific Oceans). The colors are consistent with Figure 2.

of older waters with younger ones close to the surface from the artificial upwelling. The expectations based on previous studies (e.g., Toggweiler et al. (2019)) are that upwelling regions and eastern boundaries are regions where Carbon-14 gets reset to what is in the atmosphere; Carbon-14 decreases when the Southern Ocean overturning slows there. Under artificial upwelling, salinity experiences variable change, but generally decreases at higher latitudes and increases at lower latitudes. Temperature generally increases; as a result of this and changes in thermocline ventilation, artificial upwelling does little to deter deoxygenation. Nitrate and phosphate generally increase but can decrease in high-latitude or coastal regions as well as at intermediate depths, unlike total carbon, which increases wherever it changes (primarily in locations within the mixed layer and where the mean age changes below the mixed layer). Changes in alkalinity are variable but generally decrease in the upper-ocean and at higher latitudes and increase at lower latitudes, particularly at deeper depths (Figure 6). This is just one of the GeoMIP scenarios, so we next briefly discuss (but do not show) changes in the other ones.

The dominant features of each GeoMIP scenario (not shown) include salinity decreasing in high-latitude regions, salinity increasing in lower-latitude regions, mean ages increasing, oxygen decreasing, temperature increasing, and total carbon increasing. Ocean alkalinity generally has variable change across GeoMIP scenarios, but in the ocean alkalinity enhancement

https://doi.org/10.5194/egusphere-2026-2679
Preprint. Discussion started: 21 May 2026

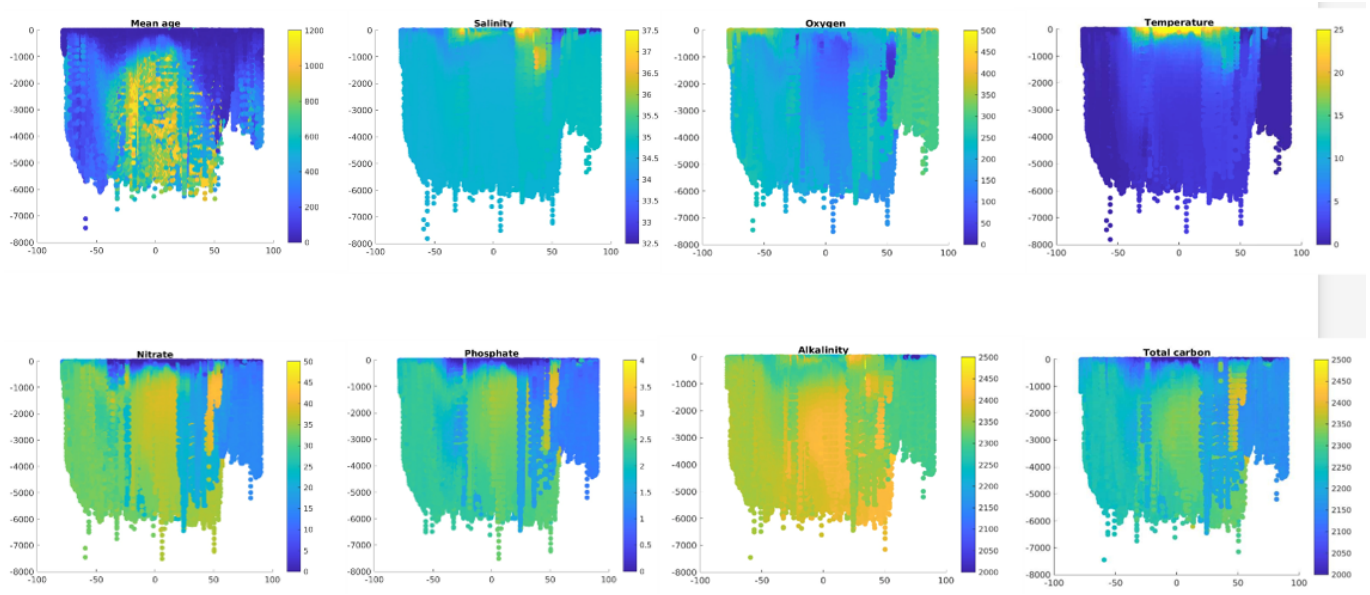

Figure 5. Control simulation state variables in the GeoMIP archive's artificial upwelling scenario at locations and depths where samples are available to compare with GLODAPv2-based estimates of calcium carbonate dissolution rates from Sulpis et al. (2021).

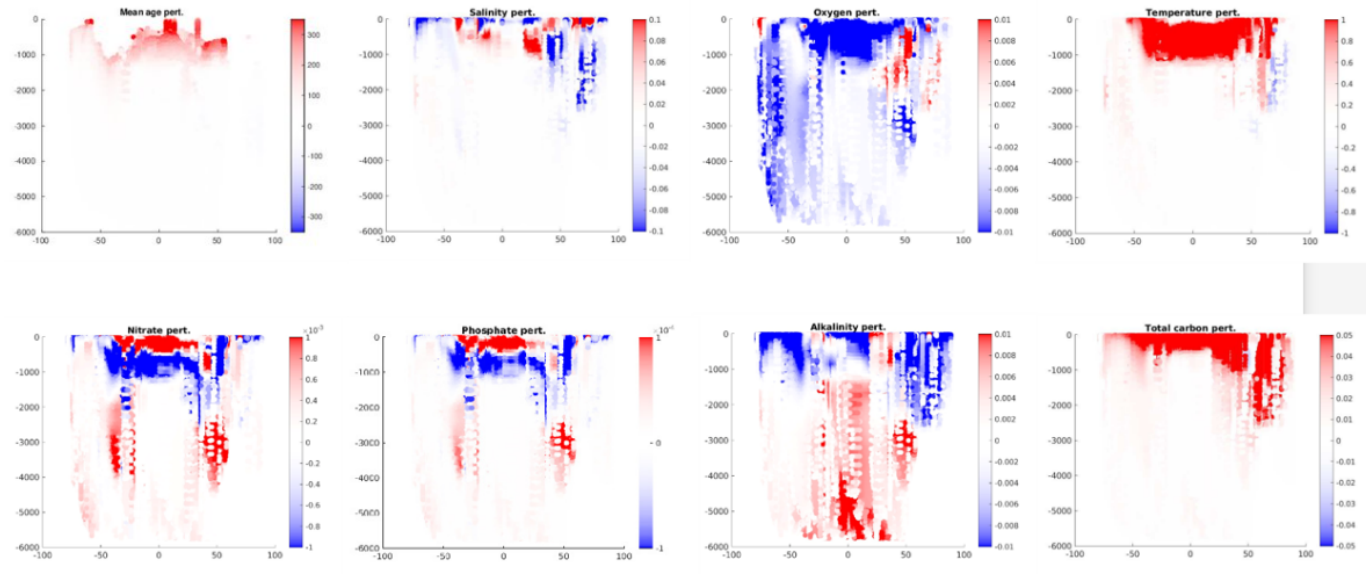

Figure 6. Perturbations to the state variables in the artificial upwelling scenario shown in Figure 5 at locations and depths where samples are available to compare with GLODAPv2-based estimates of calcium carbonate dissolution rates from Sulpis et al. (2021).

https://doi.org/10.5194/egusphere-2026-2679
Preprint. Discussion started: 21 May 2026

scenario, ocean alkalinity generally increases. The only scenario where total carbon generally decreases is the one with iron fertilization in the Southern Ocean, in which changes in each other variable are generally muted except for large increases in nitrate and phosphate in the Southern Ocean. The scenarios with the largest gain in total carbon are the ones with macroalgae farming and sinking with complete or partial remineralization. The primary difference between these macroalgae farming and sinking scenarios is that the one with complete remineralization has a decrease in nitrate while the one with partial remineralization has an increase in nitrate. Changes in oxygen and associated factors under these GeoMIP scenarios are discussed in more detail in Oschlies et al. (2025).

Each region experiences different calcium carbonate dissolution rate changes, depending on the GeoMIP scenario, and the subpolar North Atlantic is chosen here just as an example (Figure 7). Each scenario generally decreases the calcium carbonate dissolution rate, but to varying degrees. The artificial upwelling scenario, for example, assuages the dissolution rates by the least amount, whereas macroalgae farming with sinking and partial remineralization has the greatest impact on reducing the dissolution rates. Recall that the primary difference between the scenarios with macroalgae farming with sinking and either partial or complete remineralization is related to changes in nitrate (not shown). This translates into a small but noticable difference in the calcium carbonate dissolution rates.

To highlight the influence of mean age changes on calcium carbonate dissolution rates in the GeoMIP scenarios, we focus on three regions (subpolar North Atlantic, subtropical South Atlantic, and Southern Oceans) in the artificial upwelling scenario (Figure 8) with and without accounting for mean age changes. The calcium carbonate dissolution rates are reduced to nearly zero in the Southern Ocean and to a lesser extent in the subpolar North Atlantic Ocean when mean age changes are accounted for, whereas the changes primarily due to salinity only lead to modest reductions in the calcium carbonate dissolution rate without mean age changes. The calcium carbonate dissolution rates remain relatively unchanged below about 1250 dbar in the subtropical South Atlantic and Southern Oceans, even with mean age perturbations.

A comparison between the CMIP6 SSP5-8.5 scenario (Figure 2) and GeoMIP artificial upwelling scenario (Figure 9) is instructive here. All three regions considered in the CMIP6 SSP5-8.5 scenario (subtropical and subpolar North Atlantic and Indian Oceans) experience larger changes than the same regions over the same period in the GeoMIP artificial upwelling scenario. In fact, the calcium carbonate dissolution rates decrease, often by very little but decrease nevertheless, in the GeoMIP artificial upwelling scenario, whereas the dissolution rates can increase by a factor of two or more in the CMIP6 SSP5-8.5 scenario. Three other regions (Subpolar North Pacific, Equatorial Pacific, and Southern Oceans) are also shown in Figure 9 to demonstrate that the calcium carbonate dissolution rates also change very little and typically do not increase elsewhere in the ocean. The mean age perturbation is the dominant cause of the changes seen in the GeoMIP artificial upwelling scenario, with the salinity perturbation secondary (Figure 10), much like in the CMIP6 SSP5-8.5 scenario (Figures 3-4). If regions shallower than 1000 meters are masked out, our results look very similar.

These comparisons can be seen more clearly in Figure 11, which shows the range of calcium carbonate dissolution rate estimates across different scenarios for each biome. For each biome, the higher end of each envelope shown is always that of the CMIP6 scenario. The lower end of each envelope shown is often, but not always, that associated with the macroalgae farming with sinking and partial remineralization GeoMIP scenario. In the Southern Ocean, for example, macroalgae farming

https://doi.org/10.5194/egusphere-2026-2679
Preprint. Discussion started: 21 May 2026

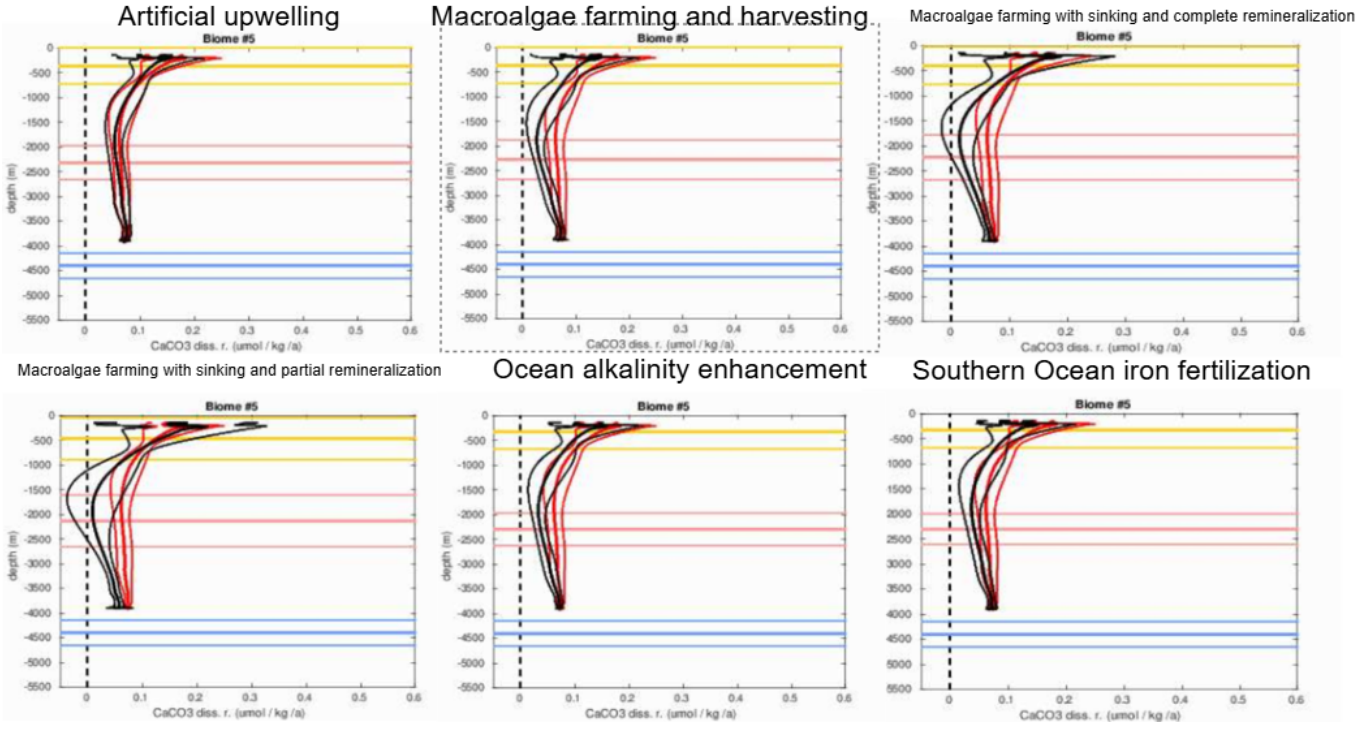

Figure 7. Calcium carbonate dissolution rates in the subpolar North Atlantic under six different GeoMIP scenarios with perturbations in temperature (T), salinity (S), age (Age), dissolved oxygen concentrations (O_2), nitrate concentrations (Nitrate), phosphate concentrations (Phosphate), alkalinity (Alk), and total carbon content (TCO_2) by adding the difference in those variables over the average of the final 30 years of GeoMIP output for each scenario minus the first 30 years of the same models to the GLODAPv2-equivalent variables at the locations where they have been sampled. Shown in black are the perturbed estimates with one standard deviation and shown in red are the initial GLODAPv2-derived estimates from Sulpis et al. (2021). The horizontal yellow line is the saturation depth of Mg calcites, the horizontal red line is the saturation depth of aragonite, and the horizontal blue line is the saturation depth of calcite in the perturbed (GeoMIP-based) estimate corresponding to the black curves.

with sinking and partial remineralization is the only geoengineering technique that increases calcium carbonate dissolution rates. Both subtropical Atlantic Ocean regions have calcium carbonate dissolution rates that can be different by an order of magnitude, depending upon the climate scenario. The North Pacific Ocean, equatorial Atlantic Ocean, and Indian Ocean, on the other hand, are not very sensitive to a given climate scenario.

To understand our results better, we show the sensitivity of the calcium carbonate dissolution rates to mean age and salinity perturbations for two different depth levels (Figure 12): one around 300 dbar (because the surface will always have a mean age of zero) and one at the seafloor. A change in salinity always decreases the calcium carbonate dissolution rate at 300 dbar, but the extent of the decrease changes according to the concomitant mean age perturbation in some regions more than others. For example, the subtropical North Atlantic and Indian Oceans have a very pronounced dependence on both factors at 300 dbar.

https://doi.org/10.5194/egusphere-2026-2679
Preprint. Discussion started: 21 May 2026

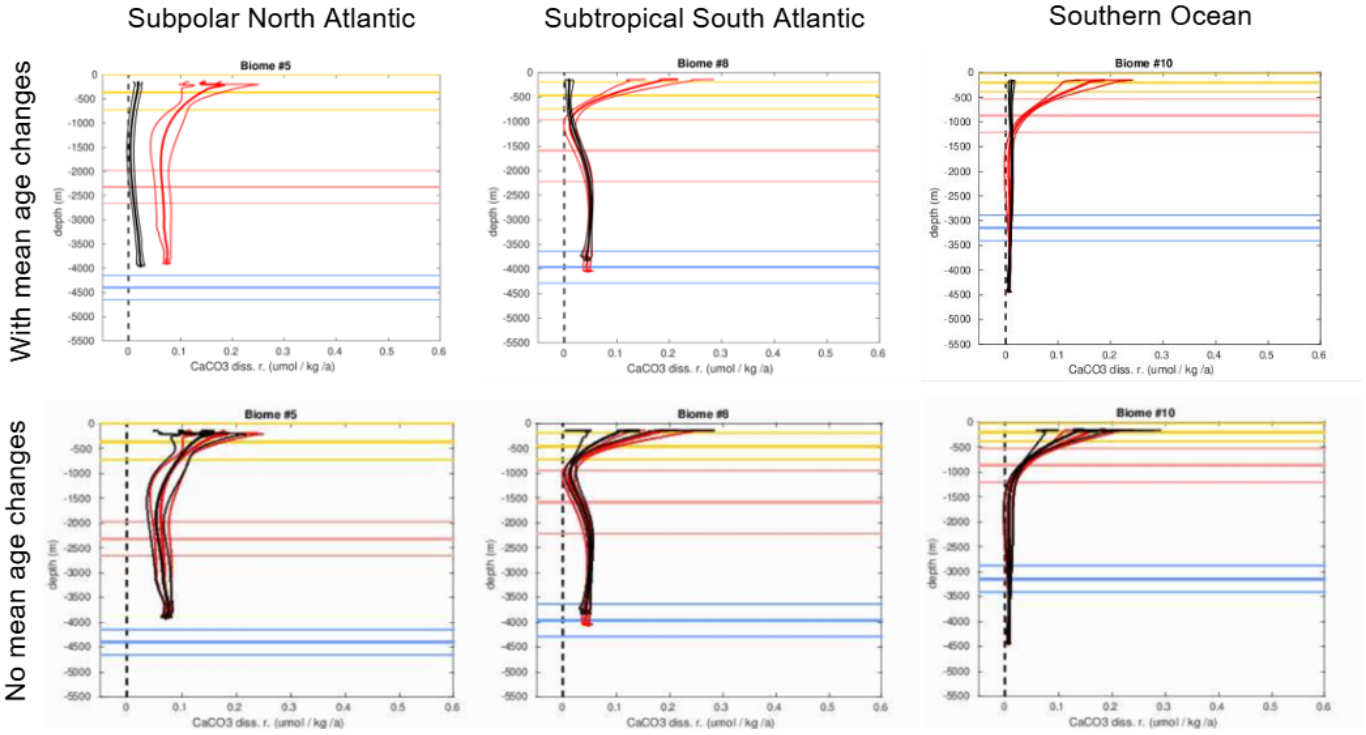

Figure 8. Calcium carbonate dissolution rates for different biomes (Fay and McKinley , 2014) or geographic regions (#10 is the Southern Ocean, #8 is the subtropical South Atlantic, and #5 is the subpolar North Atlantic) under the artificial upwelling GeoMIP scenario with perturbations in temperature (T), salinity (S), age (Age), dissolved oxygen concentrations (O_2), nitrate concentrations (Nitrate), phosphate concentrations (Phosphate), alkalinity (Alk), and total carbon content (TCO_2) (top three panels) and without the perturbations in Age but with perturbations in each of the other seven variables (bottom three panels). Here, the perturbation to the mean age is calculated from Carbon-14 via the empirical relationship described in the main text. The colors are consistent with Figure 7.

There is generally a symmetric response to the sign of the salinity perturbation in the subtropical Atlantic Ocean basins and South Pacific Ocean basins. There is a particularly pronounced asymmetry in the response to the sign of the salinity perturbation in the remaining regions. The general pattern of sensitivity is more difficult to discern at the seafloor, with the exception of the subpolar North Atlantic Ocean and the Southern Ocean, which have the greatest connectivity (smallest mean ages) to the surface. The calcium carbonate dissolution rates can be altered by nearly an order of magnitude by altering the salinity, particularly near the surface, but salinity perturbations aren't as large in the CMIP6/GeoMIP output as the ones considered in Figure 12.

https://doi.org/10.5194/egusphere-2026-2679
Preprint. Discussion started: 21 May 2026

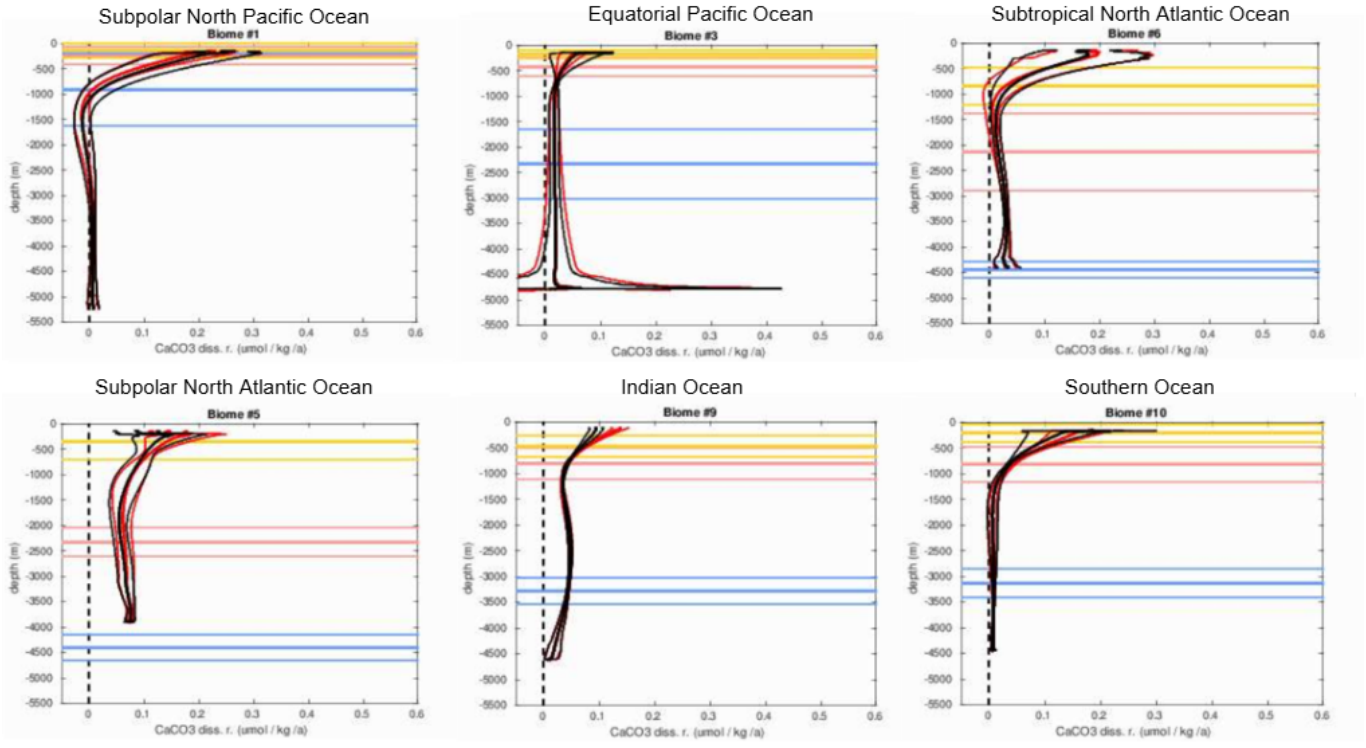

Figure 9. Calcium carbonate dissolution rates for different biomes (Fay and McKinley , 2014) or geographic regions (#10 is the Southern Ocean, #9 is the Indian Ocean, #6 is the subtropical North Atlantic, #5 is the subpolar North Atlantic, #3 is the equatorial Pacific, and #1 is the subpolar North Pacific Oceans) under the artificial upwelling GeoMIP scenario with perturbations in only salinity (S). The colors are consistent with Figure 7.

4 Direct vs indirect climate consequences

There are direct and indirect impacts of accounting for the presence of sediments on the physical ocean state of the future, neither of which is currently accounted for in coupled climate models. For instance, previous studies have suggested that more than two-thirds of the variability in marsh accretion rates can be explained by spring tidal range and suspended sediments (Coleman et al. , 2022) and there are considerable seasonal variations in seabed thickness due to freezing and thawing (Normandeau et al. , 2025). Suspended sediments in estuaries have been shown to have an impact on stratification and therefore on steric sea level (Geyer , 1993; Becker et al. , 2018; Lu et al. , 2020; Zhu et al. , 2021; Bailey et al. , 2024; Rojas et al. , 2025), but the influence of sediments on steric sea level in regions outside of estuaries in the global ocean has largely been ignored. It would be reasonable to assume that suspended sediments might also have a large impact on steric sea levels in the deltas of the world's largest rivers and nearby coasts, so we examine this next.

There are well-established methods to locally derive total suspended matter (TSM) from remotely sensed ocean color data (e.g., Li et al. (2020); Dethier et al. (2020)), which we assume has the same density and concentration as suspended sediment

https://doi.org/10.5194/egusphere-2026-2679
Preprint. Discussion started: 21 May 2026

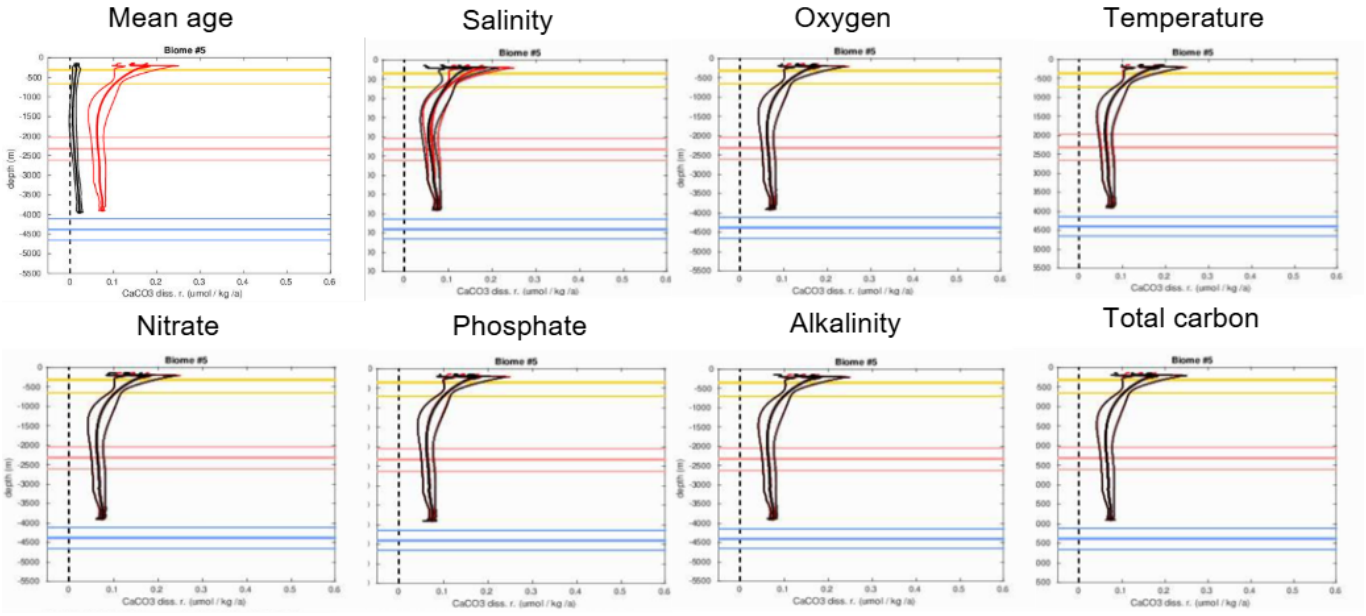

Figure 10. Calcium carbonate dissolution rates in the subpolar North Atlantic under the artificial upwelling GeoMIP scenario with perturbations in each of the state variables: temperature (T), salinity (S), age (Age), dissolved oxygen concentrations (O_2), nitrate concentrations (Nitrate), phosphate concentrations (Phosphate), alkalinity (Alk), and total carbon content (TCO_2), one at a time. The colors are consistent with Figure 7.

concentrations (SSCs) for the purpose of our back-of-the-envelope calculations. We recognize that there is calcium carbonate that is not 40% of sediment in near-coastal areas but assume that the TSM is all sediment. The impacts of SSCs on density are calculated according to $\rho_{SSC} = \text{SSC} \times (\rho_s - \rho_{ref})/\rho_s$ where $\rho_s = 2650$ kg m^{-3} and $\rho_{ref} = 999.972$ kg m^{-3} in freshwater (Do et al. , 2025). TSM (or SSC) can be calculated using a neural network algorithm (TSM$_{NN}$) using Sentinel-3a/Ocean and Land Colour Instrument (OLCI) retrievals (Yu et al. , 2022), which is the data source we use for the present study. The influence of SSC on steric sea level depends upon ρ_{ref}, which can range from about 1020 kg m$^{\breve{}3}$ to 1030 kg m^{-3} in river deltas, so we use a value of about $0.61 = (\rho_s - \rho_{ref})/\rho_s$ to scale SSC with. We calculate bottom pressure by integrating ρ times the gravitational constant over pressure. We compute steric sea level using the TEOS-10 package (McDougall et al. , 2012) but when the specific volume anomaly, $\alpha = 1/\rho$, relative to a reference value, α_{ref}, is calculated, we use $1/(1/\alpha + \rho_{SSC}) - 1/(1/\alpha_{ref} + \rho_{SSC})$ to account for SSC.

Using this formulation, typical values (2-3 kg m^{-3} for the EUMETSAT OLCI Sentinel-3 full colour TSM$_{NN}$ product (via EUMDAC ©EUMETSAT [2026]), and profiles from the World Ocean Database (2023) (Garcia et al. , 2026), we calculate the impact of SSC on steric sea level and (hydrostatic) bottom pressure. We find that observed TSM$_{NN}$ typically has a <0.1% impact on steric sea level and <0.5% impact on bottom pressure near the Amazon River delta. SSC always a larger impact on bottom pressure than steric sea level because the integrand to calculate the former is linear in density whereas the integrand

https://doi.org/10.5194/egusphere-2026-2679
Preprint. Discussion started: 21 May 2026

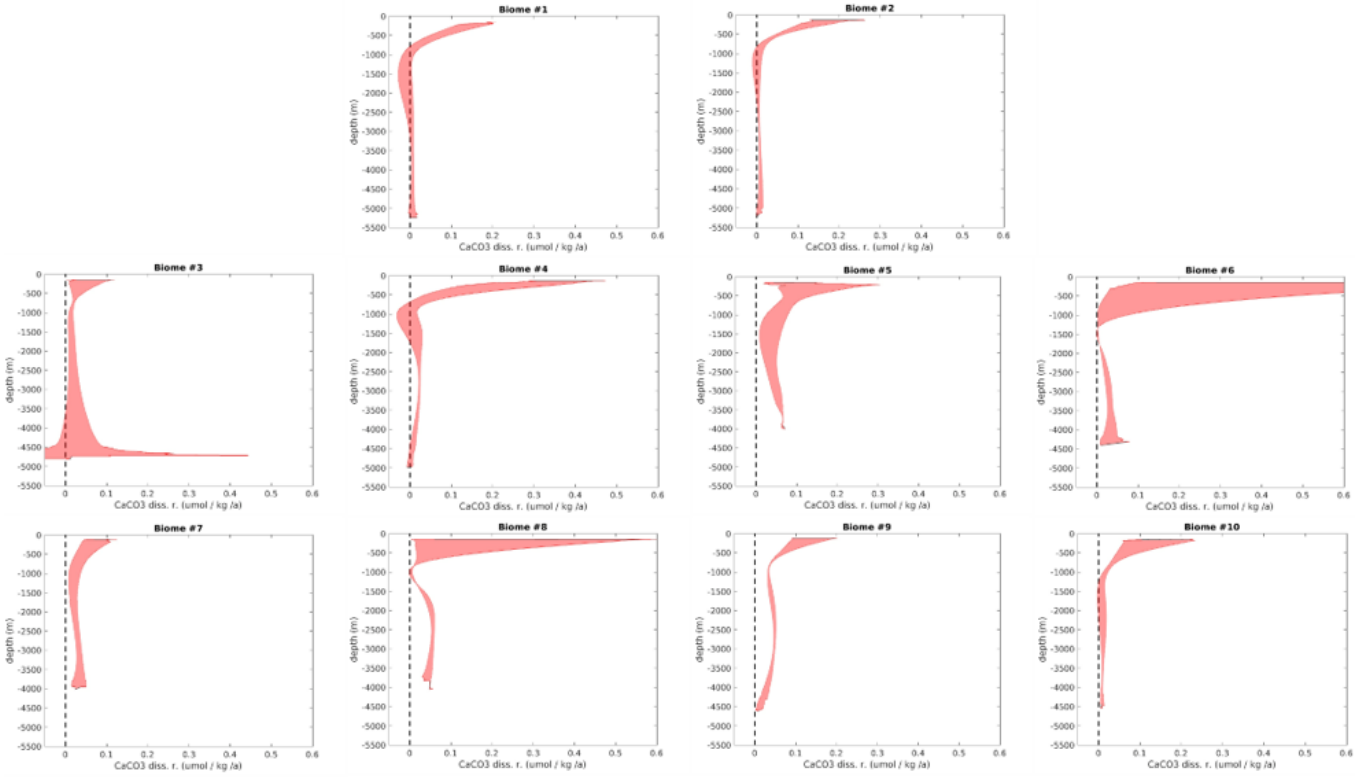

Figure 11. The ranges of calcium carbonate dissolution rates for different biomes (Fay and McKinley , 2014) or geographic regions (#1 is the subpolar North Pacific Ocean, #2 is the subtropical North Pacific Ocean, #3 is the equatorial Pacific Ocean, #4 is the subtropical South Pacific Ocean, #5 is the subpolar North Atlantic Ocean, #6 is the subtropical North Atlantic, #7 is the equatorial Atlantic Ocean, #8 is the subtropical South Atlantic Ocean, #9 is the Indian Ocean, and #10 is the Southern Ocean) under the CMIP6 with perturbations in temperature (T), salinity (S), age (Age), dissolved oxygen concentrations (O_2) and GeoMIP scenarios with perturbations in temperature (T), salinity (S), age (Age), dissolved oxygen concentrations (O_2), nitrate concentrations (Nitrate), phosphate concentrations (Phosphate), alkalinity (Alk), and total carbon content (TCO_2). Here, the perturbation to the mean age in two of the GeoMIP scenarios is calculated from Carbon-14 via the empirical relationship described in the main text. The lower bound is 1.645 times the standard deviation of the Monte Carlo estimates lower than the mean of the Monte Carlo estimates within each bin for each biome. Similarly the upper bound is 1.645 times the standard deviation of the Monte Carlo estimates higher than the mean of the Monte Carlo estimates within each bin for each biome.

to calculate the latter is inverse linear in density. The SSC would need to be more than 150 kg m^{-3} and 700 kg m^{-3} to have a 10% impact on local bottom pressure and on local steric sea level, respectively, near the Amazon River delta. In regions where we do not have historical profile data, such as along the coasts and in multiple river deltas, values of SSC regularly exceed 300 kg m^{-3} (Figure 13), so SSC can have a direct non-negligible impact on local bottom pressure and, to a lesser extent, on local steric sea level in these regions. Non-negligible impacts occur in the Amazon River delta region as well as some other locations where profile data exist, such as in the vicinity of the Ganges and Brahmaputra Rivers and along many coasts. Note that there

https://doi.org/10.5194/egusphere-2026-2679
Preprint. Discussion started: 21 May 2026

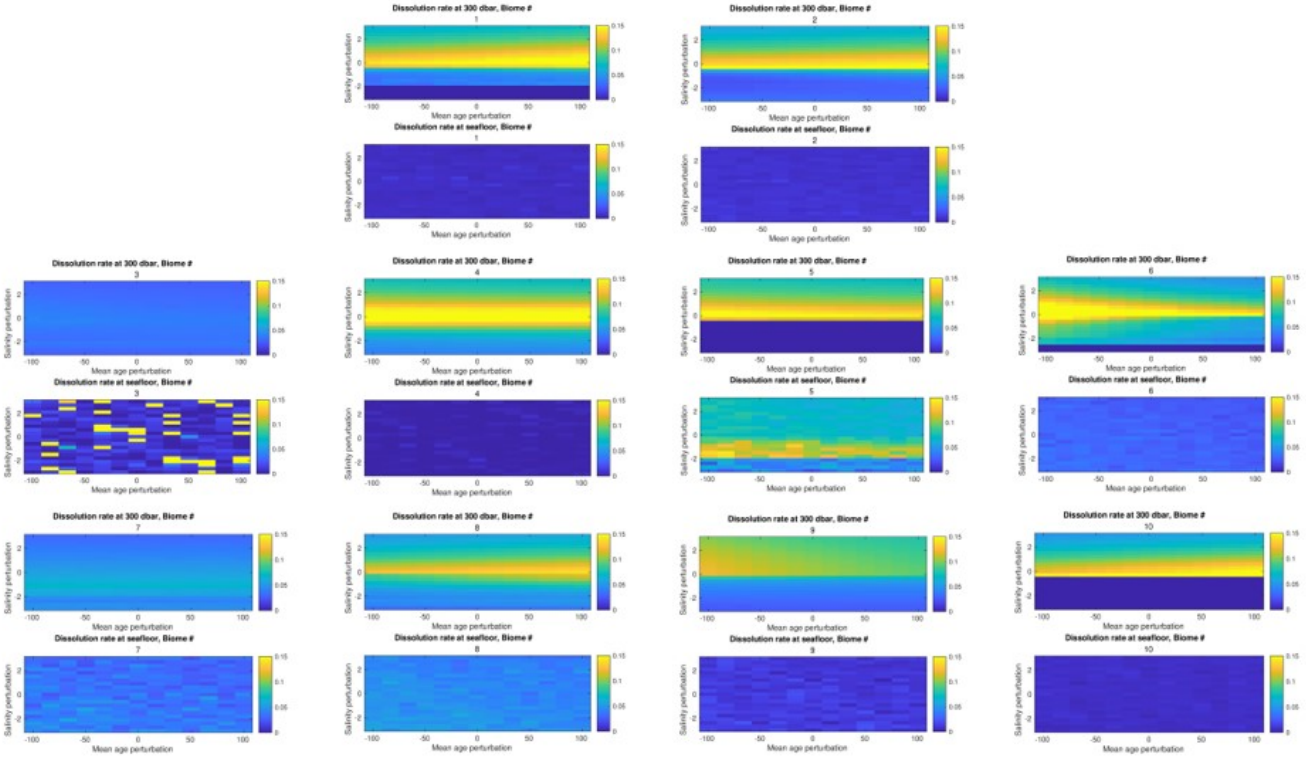

Figure 12. The mean age-salinity phase space of calcium carbonate dissolution rates for a range of -100 to 100 years and -3 to 3 PSU perturbations to the GLODAPv2-based estimates of Sulpis et al. (2021) for each of the ten biomes (Fay and McKinley , 2014). Shown are two example depth levels for each biome: one nearest to the sea surface (top) and one at the seafloor (bottom).

are small-scale feature apparent in Figure 13 that can be interpreted as large SSC (> 300 kg m$^{\breve{}3}$) outside of the Ganges and Brahamputra River deltas, so when those values are co-located with World Ocean Database profiles, we find a 10% impact on bottom pressure and a few percent impact on steric sea level. However, these small-scale features can be sensitive to the application of particular flags in the data.

Given the significant direct impact of the presence of SSC > 300 kg m$^{\breve{}3}$ along the coasts and in multiple river deltas, an increase in the calcium carbonate dissolution rate by a factor of two (e.g., in the subtropical North Atlantic Ocean) would then also have a non-negligible impact on steric sea level, which would act as a contraction effect. The mean age of waters with high SSC along the coasts will not significantly change, but salinity can be very different, suggesting that the calcium carbonate dissolution rates may change along the coasts in the future. However, we cannot verify this using the CMIP6 and GeoMIP model output because they are not sufficiently high-resolution to provide insights about the magnitude.

There are a couple of studies whose findings may be interpreted differently, considering the potential importance of SSC along the coasts. First, it is unclear whether these findings validate the interpretation of the gravimetric signals found in the delta of the Amazon River in a previous study (Oh et al. , 2025) as sediment. These signals could instead, or in addition, be

https://doi.org/10.5194/egusphere-2026-2679
Preprint. Discussion started: 21 May 2026

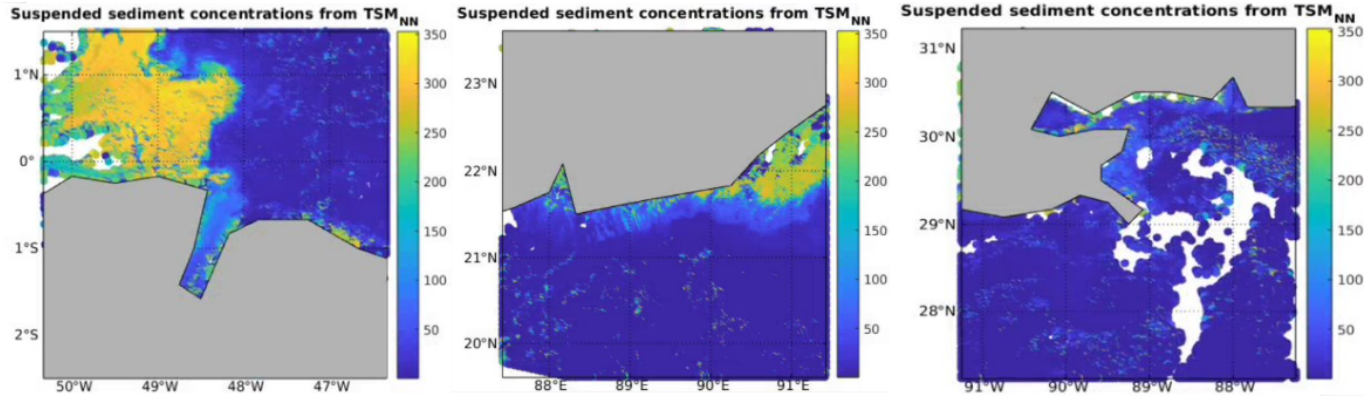

Figure 13. Three regional examples of SSC from Level-2 Sentinel-3a OLCI TSM$_{NN}$: Amazon River delta (May 2-3, 2024), Ganges/Brahmaputra River deltas (October 8-9, 2024), and Mississippi River delta (August 23-24, 2024). The flags used here include 'LAND' and 'CLOUD' but can additionally include, for instance: 'CLOUD_AMBIGUOUS', 'CLOUD_MARGIN', 'INVALID', 'COSMETIC', 'SATURATED', 'SUSPECT', 'HISOLZEN', 'HIGHGLINT', 'SNOW_ICE', 'AC_FAIL', 'WHITECAPS', and 'ADJAC'e.

related to the flux of terrestrial water storage (Chandanpurkar et al. , 2025). Second, the finding that wave-induced set-up and swash effects are important to account for in coastal sea level budgets (Melet et al. , 2018, 2020) could at least partially be explained by the significance of SSC. SSC can significantly change during storm events (Wang et al. , 2024; Guillén et al. , 2024), and these same events can cause extreme coastal sea levels. However, it is beyond the scope of the present study to quantify these effects.

The indirect effect of accounting for sediments and calcium carbonate dissolution on future sea level via changes in the carbon budget may be globally and locally significant. Using the empirical framework employed by Williams et al. (2012), we estimate that a 10% difference in carbon dioxide outgassing (an upper bound on what would happen with a 10% increase in ocean carbon inventory) would lead to a factor of three increase in equilibrium carbon dioxide level (see their Eq 5) and 10% increase in radiative heat flux at the sea surface and sea surface temperature at equilibrium (see their Eqs 6 and 8). This would translate into a 21% increase in sea level at equilibrium (see their Eq 10). However, a more complex interplay of physical and biogeochemical processes, including the representation of calcium carbonate dissolution could significantly modify these back-of-the-envelope global estimates (Gillett , 2023) and there will be large variations on regional scales (Nauels et al. , 2025). For instance, turbidity currents are known to play a role in the redistribution and preservation of carbon in deep-sea sediments (Nworie et al. , 2026). Predicting the oceanic sources and sinks of carbon dioxide and whether the ocean will continue to be a sink will be critical to understanding the future physical ocean state and these crude calculations suggest that coupled climate simulations may need to account for sediment dynamics and calcium carbonate dissolution (e.g., Ye et al. (2025)).

https://doi.org/10.5194/egusphere-2026-2679
Preprint. Discussion started: 21 May 2026

5 Conclusions

We investigated the range of possible future calcium carbonate dissolution rates and the dominant factors that determine their future changes. The biome/region with the largest future calcium carbonate dissolution rate changes in CMIP6 output is the subtropical North Atlantic Ocean, where the dominant driver of future calcium carbonate dissolution rate changes is salinity. The effects of salinity and mean age perturbations each primarily drive future calcium carbonate dissolution rate changes in the subpolar North Atlantic Ocean in CMIP6 output, but mean age dominates. In the absence of mean age changes, artificial upwelling is the only geoengineering technique that lessens the calcium carbonate dissolution rates in the Indian Ocean, but artificial upwelling is the least effective geoengineering technique to reduce calcium carbonate dissolution rates in the subpolar North Atlantic Ocean. Also without mean age changes, macroalgae farming with sinking and partial remineralization is the only geoengineering technique that increases calcium carbonate dissolution rates in the Southern Ocean, but is generally the most effective geoengineering technique to assuage calcium carbonate dissolution rates. Iron fertilization in Southern Ocean and ocean alkalinity enhancement are the two scenarios that are least effective at assuaging calcium carbonate dissolution rates in the subtropical South Atlantic Ocean. The effect of adding alkalinity in the ocean alkalinity enhancement experiment is not what reduces the calcium carbonate dissolution rates; it is the changes in mean age and salinity. The range of calcium carbonate dissolution rates can be an order of magnitude in regions such as the two subtropical Atlantic Ocean basins, so the future of calcium carbonate dissolution rates strongly depends on our future emissions pathway.

There are some shortcomings in our diagnostic approach using model output from future climate simulations, which can be improved in future studies, but the present study also points to future research directions. Because of our diagnostic approach with ocean tracer variables, we do not have sufficient information to accurately calculate calcium carbonate dissolution changes associated with coral reefs and other species on the continental shelves. Further, akin to the difference between available oxygen utilization and total oxygen utilization (e.g., Sulpis et al. (2023)), a caveat of the present study is that we have not properly accounted for cross-isopycnal transports and mixing to estimate the calcium carbonate dissolution rates. However, one benefit of the method we used to perform this study is that it allows us to understand the factors of first order importance under climate change scenarios to future calcium carbonate dissolution rate behavior. We did not discuss the changes in the sinking fluxes of sediments because they change very little; only in the Indian Ocean are they visually different under the climate change scenarios and those decrease by a small amount. Also, our inferred ages from Carbon-14 can change dramatically due to the inapplicability of our crude empirical formula for relatively young waters, which can lead to large changes in calcium carbonate dissolution rate changes. This was highlighted with results using the artificial upwelling scenario. In the absence of mean ages for the GeoMIP scenarios, we don't know the full range of possible calcium carbonate dissolution rates, but we have shown how sensitive these estimates can be to mean age changes. Also, in the absence of in situ measurements in river deltas and nearby coasts, we don't know how much accounting for suspended sediments, let alone how calcium carbonate dissolution rate changes, will impact future sea level budgets in these regions, but we argue that these factors can be non-negligible. One suggestion we can make based on the sensitivities of calcium carbonate dissolution rates to various perturbed factors in the future is that geoengineering techniques should be chosen such that changes in ocean ventilation and salinity are minimized.

https://doi.org/10.5194/egusphere-2026-2679
Preprint. Discussion started: 21 May 2026

Future studies will investigate the direct and indirect impacts of these changes more quantitatively in terms of the carbon budget, sea level, and other factors.

Code and data availability. The CMIP6 data were downloaded from the link provided in Guo et al. (2025). The GeoMIP data were downloaded from the link provided in Oschlies et al. (2025). The observationally-derived data (e.g., GLODAPv2 and mean ages) were downloaded from the link provided in Sulpis et al. (2021). The Matlab code used and the results generated using the above data with this code are available here: https://zenodo.org/10.5281/zenodo.19683268

Author contributions. D.T. conceived of the idea, executed the analysis, and wrote up the manuscript.

Competing interests. No competing interests are declared.

Acknowledgements. The author thanks Olivier Sulpis for the code used as a basis for most of the calculations in this study and some feedback.
310 DT was supported by the NERC AtlantiS project (NE/Y005589/1).

https://doi.org/10.5194/egusphere-2026-2679
Preprint. Discussion started: 21 May 2026

References

Archer, D., M. Eby, V. Brovkin, A. Ridgwell, L. Cao, U. Mikolajewicz, K. Caldeira, K. Matsumoto, G. Munhoven, A. Montenegro, K. Tokos, 2009: Atmospheric lifetime of fossil fuel carbon dioxide. Annu. Rev. Earth Planet. Sci. 37, 117–134.

Bailey, T., L. Ross, H. M. Schuttelaars, D. S. van Maren, 2024: Impacts of the Seasonal Migration of an Estuarine Turbidity Maximum on Local Hydrodynamics and Mixing in the Ems Estuary. Estuaries and Coasts, 48, 19, https://doi.org/10.1007/s12237-024-01438-4

Becker, M., C. Maushake, C. Winter, 2018: Observations of Mud-Induced Periodic Stratification in a Hyperturbid Estuary. Geophysical Research Letters, 45, 5461–5469. https://onlinelibrary.wiley.com/doi/pdf/10.1029/2018GL077966

Carter, B. R., J. R. Toggweiler, R. M. Key, J. L. Sarmiento, 2014: Processes determining the marine alkalinity and calcium carbonate saturation state distributions. Biogeosciences 11, 7349–7362.

Chandanpurkar, H. A., J. S. Famiglietti, K. Gopalan, D. N. Wiese, Y. Wada, K. Kakinuma, J. T. Reager, F. Zhang, 2025: Unprecedented continental drying, shrinking freshwater availability, and increasing land contributions to sea level rise. Sci. Adv., 11, eadx0298. https://doi.org/10.1126/sciadv.adx0298

Cohen, S., J. Syvitski, T. Ashley, R. Lammers, B. Fekete, H.-Y. Li, 2022: Spatial trends and drivers of bedload and suspended sediment fluxes in global rivers. Water Resources Research, 58, e2021WR031583. https://doi.org/10.1029/2021WR031583

Coleman, D.J., M. Schuerch, S. Temmerman, G. Guntenspergen, C. G. Smith, M. L. Kirwan, 2022: Reconciling models and measurements of marsh vulnerability to sea level rise. Limnol Oceanogr Lett, 7: 140-149. https://doi.org/10.1002/lol2.10230

Dethier, E. N., C. E. Renshaw, F. J. Magilligan, 2020: Toward improved accuracy of remote sensing approaches for quantifying suspended sediment: Implications for suspended-sediment monitoring. Journal of Geophysical Research: Earth Surface, 125, e2019JF005033. https://doi.org/10.1029/2019JF005033

Do, T.-K.-A., N. Huybrechts, I. Jálon-Rojas, P. Tassi, A. Sottolichio, 2025: Three-dimensional numerical modeling of sediment transport in a highly turbid estuary with pronounced seasonal variations. International Journal of Sediment Research, 40, 333–347, 495. https://doi.org/10.1016/j.ijsrc.2024.12.003

Fay, A. R., G. A. McKinley, 2014: Global open-ocean biomes: mean and temporal variability. Earth Syst. Sci. Data 6, 273–284.

Feely, R. A., C. L. Sabine, K. Lee, W. Berelson, J. Kleypas, V. J. Fabry, F. J. Millero 2004: Impact of anthropogenic CO2 on the CaCO3 system in the oceans. Science 305, 362–366.

Garcia, H., T. Boyer, S. Levitus, J. Reagan, A. Mishonov, L.-Q. Jiang, Z. Wang, C. Paver, E. Nyadjro, S. Cross, C. Bouchard, P. Hogan, O. Baranova, R. Locarnini, 2026: World Ocean Database 2023: A Foundational Data Resource for and by the Global Ocean and Coastal Communities. Sci Data 13, 613. https://doi.org/10.1038/s41597-026-06957-2

Gebbie, G., P. Huybers, 2012: The mean age of ocean waters inferred from radiocarbon observations: sensitivity to surface sources and accounting for mixing histories. J. Phys. Oceanogr. 42, 291–305.

Geyer, W. R., 1993: The importance of suppression of turbulence by stratification on the estuarine turbidity maximum. Estuaries, 16, 113–125. https://doi.org/10.2307/1352769

Gillett, N.P., 2023: Warming proportional to cumulative carbon emissions not explained by heat and carbon sharing mixing processes. Nat Commun 14, 6466. https://doi.org/10.1038/s41467-023-42111-x

Gnanadesikan, A., J. L. Russell, F. Zeng, 2007: How does ocean ventilation change under global warming? Ocean Sci. 3, 43–53.

https://doi.org/10.5194/egusphere-2026-2679
Preprint. Discussion started: 21 May 2026

Goossens, C., S. J. van deVelde, F. J. R. Meysman, 2026: A revised estimate of calcium carbonate dissolution in coastal and shelf sediments suggests large shelf exports in the marine CaCO3 cycle. Global Biogeochemical Cycles, 40, e2025GB008936. https://doi.org/10.1029/2025GB008936

Guillén, J., G. Simarro, D. Calvete, F. Ribas, A. Fernández-Mora, A. Orfila, A. Falqués, R. de Swart, A. Sancho-García, R. Durán, 2024: Sediment leakage on the beach and upper shoreface due to extreme storms. Marine Geology, 468, 107207, ISSN 0025-3227. https://doi.org/10.1016/j.margeo.2023.107207

Guo, H., W. Koeve, A. Oschlies, Y.-C. He, T. P. Kemena, L. Gerke, I. Kriest, 2025: Dual-tracer constraints on the inverse Gaussian transit time distribution improve the estimation of water mass ages and their temporal trends in the tropical thermocline. Ocean Sci. 21, 1167–1182.

Guo, H., W. Koeve, I. Kriest, I. Frenger, T. Tanhua, P. Brandt, Y. He, T. Xue, A. Oschlies, 2026: North Atlantic ventilation change over the past three decades is potentially driven by climate change. Nat Commun 17, 200. https://doi.org/10.1038/s41467-025-67923-x

Hamlington, B. D., A. S. Gardner, E. Ivins, J. T. M. Lenaerts, J. T. Reager, D. S. Trossman, E. D. Zaron, S. Adhikari, A. Arendt, A. Aschwanden, B. D. Beckley, D. P. S. Bekaert, G. Blewitt, L. Caron, H. A. Chandanpurkar, K. Christianson, R. I. Cullather, R. M. DeConto, J. T. Fasullo, T. Frederikse, J. T. Freymueller, D. M. Gilford, M. Girotto, W. C. Hammond, R. Hock, N. Holschuh, R. E. Kopp, F. Landerer, E. Larour, D. Menemenlis, M. Merrifield, J. X. Mitrovica, R. S. Nerem, I. J. Nias, V. Nieves, S. Nowicki, K. Pangaluru, C. G. Piecuch, D. R. Rounce, N.-J. Schlegel, H. Seroussi, M. Shirzaei, I. Velicogna, N. Vinogradova, T. Wahl, D. N. Wiese, M. J. Willis, 2020: Understanding of contemporary regional sea-level change and the implications for the future. Reviews of Geophysics, 59, e2019RG000672; https://doi.org/10.1029/2019RG000672

Hernandez-Cruz, B., M. Vasquez-Ortiz, C. Canet, J. Prado-Molina, 2019: Algorithm to calculate suspended sediment concentration using Landsat 8 imagery. Applied Ecology and Environmental Research, 17(3): 6549-6562. http://dx.doi.org/10.15666/aeer/1703_65496562

Jeansson, E., R. Steinfeldt, T. Tanhua, 2021: Water Mass Ages Based On GLODAPv2 Data Product (NCEI Accession 0226793) (NOAA, National Centers for Environmental Information).

Khatiwala, S., F. Primeau, M. Holzer, 2012: Ventilation of the deep ocean constrained with tracer observations and implications for radiocarbon estimates of ideal mean age. Earth and Planetary Science Letters, 325–326, 116-125, ISSN 0012-821X. https://doi.org/10.1016/j.epsl.2012.01.038

Kwon, E. Y., J. P. Dunne, K. Lee, 2024: Biological export production controls upper ocean calcium carbonate dissolution and CO2 buffer capacity. Science Advances, 10(13). https://doi.org/10.1126/sciadv.adl07

Kyryliuk, D., S. Kratzer, 2019: Evaluation of Sentinel-3A OLCI Products Derived Using the Case-2 Regional Coast Colour Processor over the Baltic Sea. Sensors (Basel), 19(16):3609. https://doi.org/10.3390/s19163609

Li, L., N. Jinren, F. Chang, Y. Yue, N. Frolova, D. Magritsky, A. G. L. Borthwick, P. Ciais, Y. Wang, C. Zheng, D. E. Walling, 2020: Global trends in water and sediment fluxes of the world's large rivers. Science Bulletin, 65(1), 62-69. https://doi.org/10.1016/j.scib.2019.09.012

Lu, T., H. Wu, F. Zhang, J. Li, L. Zhou, J. Jia, Z. Li, Y. P. Wang, 2020: Constraints of salinity- and sediment-induced stratification on the turbidity maximum in a tidal estuary. Geo-Marine Letters, 40, 765–779. https://doi.org/10.1007/s00367-020-00670-8

Ludwigsen, C. B., O. B. Andersen, B. Marzeion, J.-H. Malles, H. M. Schmied, P. Döll, C. Watson, M. A. King, 2024: Global and regional ocean mass budget closure since 2003. Nat Commun, 15, 1416. https://doi.org/10.1038/s41467-024-45726-w

McDougall, T. J., D. R. Jackett, F. J. Millero, R. Pawlowicz, P. M. Barker, 2012: A global algorithm for estimating Absolute Salinity. Ocean Science, 8, 1123-1134.

Melet, A., B. Meyssignac, R. Almar, G. Le Cozannet, 2018: Under-estimated wave contribution to coastal sea-level rise. Nature Clim Change, 8, 234–239. https://doi.org/10.1038/s41558-018-0088-y

https://doi.org/10.5194/egusphere-2026-2679
Preprint. Discussion started: 21 May 2026

Melet, A., R. Almar, M. Hemer, G. Le Cozannet, B. Meyssignac, P. Ruggiero, 2020: Contribution of wave setup to projected coastal sea level changes. Journal of Geophysical Research: Oceans, 125, e2020JC016078. https://doi.org/10.1029/2020JC016078

Molodtsov, S., I. Marinov, W. Weijer, D. DeSantis, A. Jonko, M. Veneziani, J. Lu, 2025: North Atlantic temperature and salinity changes are driven by external forcing, underestimated by CMIP6 models. npj Clim Atmos Sci 8, 332. https://doi.org/10.1038/s41612-025-01210-w

Moragoda, N., S. Cohen, 2020: Climate-induced trends in global riverine water discharge and suspended sediment dynamics in the 21st century. Global and Planetary Change, 191, 103199. https://doi.org/10.1016/j.gloplacha.2020.103199

Nauels, A., Z. Nicholls, T. Möller, T. H. J. Hermans, M. Mengel, U. Kloenne, C. Smith, A. B. A. Slangen, M. D. Palmer, 2025: Multi-century global and regional sea-level rise commitments from cumulative greenhouse gas emissions in the coming decades. Nat. Clim. Chang. 15, 1198–1204. https://doi.org/10.1038/s41558-025-02452-5

Nookala, S. R., J. G. Duan, K. Qi, J. Pacheco, S. He, 2025: Quantification of Suspended Sediment Concentration Using Laboratory Experimental Data and Machine Learning Model. Water, 17(15), 2301. https://doi.org/10.3390/w17152301

Normandeau, A., B. L. Kurylyk, E. J. Harrison, H. D. Geizer, G. Philibert, R. Way, C. L. Algar, Z. MacMillan-Kenny, J. L. Eamer, N. Van Nieuwenhove, J. B. R. Eamer, L. Pijogge, F. Cyr, I. Church, E. Oliver, M. Saunders, A. Limoges, 2025: Winter in the coastal ocean: Seasonal freezing causes seafloor expansion and contraction. Sci. Adv., 11, eadw7439. https://doi.org/10.1126/sciadv.adw7439

Nworie, C. D., Z. R. Jobe, A. Slootman, R. Venturelli, J. T. Eggenhuisen, J. J. G. Reijmer, 2026: Carbonate turbidity currents play an underappreciated role in the global carbon cycle. The Sedimentary Record, 24(1). https://doi.org/10.2110/001c.159298

Oh, E. H., K.-W. Seo, T. Jeon, J. Eom, J. Chen, C. R. Wilson, 2025: Sediment accumulation at the Amazon coast observed by satellite gravimetry. Remote Sensing of Environment, 321, 114688. https://doi.org/10.1016/j.rse.2025.114688

Oschlies, A., C. Slomp, A. H. Altieri, N. D. Gallo, M. Gregoire, K. Isensee, L. Levin, J. Wu, 2025: Potential impacts of marine carbon dioxide removal on ocean oxygen. Environmental Research Letters, 20, 073002. https://doi.org/10.1088/1748-9326/ade0d4

Rojas, C. M., L. Ross, B. J. Kaimathuruthy, I. Jalón-Rojas, A. Sottolichio, N. Huybrechts, 2025: The impact of suspended sediments on exchange flow in a macrotidal, hyperturbid estuary. Ocean Science Discussions. https://doi.org/10.5194/egusphere-2025-6311

Soriano-González, J., E. P. Urrego, X. Sòria-Perpinyà, E. Angelats, C. Alcaraz, J. Delegido, A. Ruíz-Verdú, C. Tenjo, E. Vicente, J. Moreno, 2022: Towards the Combination of C2RCC Processors for Improving Water Quality Retrieval in Inland and Coastal Areas. Remote Sens. 2022, 14, 1124. https://doi.org/10.3390/rs14051124

Sulpis, O., B. P. Boudreau, A. Mucci, C. Jenkins, D. S. Trossman, B. K. Arbic, R. M. Key, 2018: Current CaCO3 Dissolution at the Seafloor Caused by Anthropogenic CO2. Proceedings of the National Academy of Science of the USA, 115(45), 11700-11705. https://doi.org/10.1073/pnas.1804250115

Sulpis, O., E. Jeansson, A. Dinauer, S. K. Lauvset, J. J. Middelburg, 2021: Calcium carbonate dissolution patterns in the ocean. Nat. Geosci. 14, 423–428. https://doi.org/10.1038/s41561-021-00743-y

Sulpis, O., D. S. Trossman, M. Holzer, E. Jeansson, S. K. Lauvset, J. J. Middelburg, 2023: Respiration patterns in the dark ocean. Global Biogeochemical Cycles, 37, e2023GB007747; https://doi.org/10.1029/2023GB007747

Sun, X., L. Tian, H. Fang, D. E. Walling, L. Huang, E. Park, D. Li, C. Zheng, L. Feng, 2025: Changes in global fluvial sediment concentrations and fluxes between 1985 and 2020. Nat Sustain, 8, 142–151. https://doi.org/10.1038/s41893-024-01476-7

Testorf, P., C. Schannwell, M.-L. Kapsch, U. Mikolajewicz, 2026: Coupled climate-ice-sheet simulations reveal novel teleconnection between northern hemisphere ice sheets and the Antarctic ice sheet. Geophysical Research Letters, 53, e2025GL118959. https://doi.org/10.1029/2025GL118959

https://doi.org/10.5194/egusphere-2026-2679
Preprint. Discussion started: 21 May 2026

Toggweiler, J. R., E. R. M. Druffel, R. M. Key, E. D. Galbraith, 2019: Upwelling in the ocean basins north of the ACC: 1. On the upwelling exposed by the surface distribution of Δ14C. Journal of Geophysical Research: Oceans, 124, 2591–2608. https://doi.org/10.1029/2018JC014794

van deVelde, S. J., P. Vervoort, R. O. Smith, C. S. Law, K. Currie, 2026: Anthropogenically stimulated carbonate dissolution in the global shelf seafloor is potentially an important and fast climate feedback. AGU Advances, 7, e2025AV001865. https://doi.org/10.1029/2025AV001865

van Heuven, S., D. Pierrot, J. W. B. Rae, E. Lewis, D. W. R. Wallace, 2011: MATLAB Program Developed for CO_2 System Calculations (ORNL/CDIAC-105b) (DOE). https://doi.org/10.3334/CDIAC/otg.CO2SYS_MATLAB_v1.1

Wang, C., G. Yang, C. Li, C. Zhao, J. Zhu, X. Ma, 2024: The response of sediment transport and morphological evolution to storms with different characteristics. Science of The Total Environment, 946, 173987, ISSN 0048-9697. https://doi.org/10.1016/j.scitotenv.2024.173987.

Williams, R. G., P.Goodwin, A.Ridgwell, P. L.Woodworth, 2012: How warming and steric sea level rise relate to cumulative carbon emissions. Geophys. Res. Lett., 39, L19715. https://doi.org/10.1029/2012GL052771

Wu, Y., Y. Huang, T. DeVries, S. Zhang, 2025: The dominant sink of oceanic calcium carbonate occurs in undersaturated seawater. Proceedings of the National Academy of Science of the USA, 122 (43), e2507771122. https://doi.org/10.1073/pnas.250777112

Ye, Y., G. Munhoven, P. Köhler, M. Butzin, J. Hauck, Ö. Gürses, C. Völker, 2025: FESOM2.1-REcoM3-MEDUSA2: an ocean–sea ice–biogeochemistry model coupled to a sediment model. Geosci. Model Dev., 18, 977–1000. https://doi.org/10.5194/gmd-18-977-2025

Yu, X., Z. Lee, F. Shen, M. Wang, J. Wei, L. Jiang, Z. Shang, 2019: An empirical algorithm to seamlessly retrieve the concentration of suspended particulate matter from water color across ocean to turbid river mouths. Remote Sensing of Environment, 235, 111491, ISSN 0034-4257. https://doi.org/10.1016/j.rse.2019.111491

Yu, Z., J. Wang, Y. Li, C. K. Shum, B. Wang, X. He, H. Xu, Y. Xu, B. Zhou, 2022: Remote sensing of suspended sediment in high turbid estuary from sentinel-3A/OLCI: A case study of Hangzhou Bay. Front. Mar. Sci. 9:1008070. https://doi.org/10.3389/fmars.2022.1008070

Zhu, C., D. S. van Maren, L. Guo, J. Lin, Q. He, Z. B. Wang, 2021: Effects of Sediment-Induced Density Gradients on the Estuarine Turbidity Maximum in the Yangtze Estuary. Journal of Geophysical Research: Oceans, 126, e2020JC016 927, 615. https://onlinelibrary.wiley.com/doi/pdf/10.1029/2020JC016927